Air Quality, Atmosphere & Health (2020) 13:435–446
https://doi.org/10.1007/s11869-020-00811-z

Health-relevant ground-level ozone and temperature events under future climate change using the example of Bavaria, Southern Germany

Elke Hertig [1]

Received: 17 December 2019 / Accepted: 5 March 2020 / Published online: 19 March 2020
© The Author(s) 2020

Abstract

Relationships of larger scale meteorological predictors with ground-level daily maximum ozone (O_{3max}) and daily maximum air temperature (T_{max}) for stations in Bavaria were analysed. O_{3max} and T_{max} as well as threshold exceedances of these variables were assessed under the constraints of ongoing climate change until the end of the twenty-first century. Under RCP8.5 scenario conditions, a substantial increase of T_{max} in the months from April to September arose, with a mean value of 5 K in the period 2081–2100 compared with the historical period 1986–2005. Statistical downscaling projections pointed to a mean O_{3max} rise of 17 μg/m^3. The frequency of threshold exceedances showed also large changes. Hot days may occur in the future at about 30% of all days. Exceedances of $O_{3max} > 100$ μg/m^3 were projected to increase to about 40% of all days at urban traffic sites and up to about 70% in the rural regional background. Days with $O_{3max} > 120$ μg/m^3 occurred still at about 20% of all days at urban traffic sites and at about 45% in rural regional background locations. With respect to combined $T_{max} > 30$ °C and $O_{3max} > 100$ μg/m^3 events in the future, an occurrence of such events at about 27–29% of all days in the summer months from April to September was assessed. The increases were mainly associated with the strong temperature rise until the end of the century. In summary, the projected T_{max} and O_{3max} changes point to a considerable increased health burden in Bavaria until the end of the century, resulting from strong changes of both variables and their associated individual and combined impact on human health.

Keywords Regional climate change · Air temperature · Ground-level ozone · Human health · Statistical downscaling

Introduction

From the combination of demographic changes (urbanisation, increase of the share of older people in total population), climate change (increase of mean and extreme temperature) and local urban effects (urban heat island, concentration of air pollution), considerable health risks related to climate and air substances emerge. A specific concern applies to ground-level air temperature and ozone (O_3) concentrations, due to the physical relationships between these variables, the single and combined effects of both variables on human health and the anticipated substantial changes in the scope of climate change.

Temperature extremes like hot days and heat waves can have a negative impact on human health and prolonged exposure to high air temperature can cause heat-related diseases like heat exhaustion and heat stroke. Epidemiological studies have shown that high air temperatures are related to increased mortality (Hajat and Kosatky 2010). Heat exposure was found to be associated with increased risk of cardiovascular, cerebrovascular and respiratory mortality (Song et al. 2017). However, the authors also noted that health effects of temperature depend on the definition of indicators and thresholds and that definitions of temperature exposure at the regional level are necessary. With respect to thermal load, an official warning is issued by the German Weather Service when the apparent temperature exceeds 32 °C. Also, the definition of a "hot day" with maximum temperature >30 °C is frequently used in studies (e.g. Vescovi et al. 2005).

Exposure to ground-level O_3 can also have significant health impacts. Ground-level O_3 is a secondary air substance, which is primarily built by photochemical reactions under solar radiation with the involvement of precursor gases including nitrogen oxides, carbon monoxide, methane and non-

Electronic supplementary material The online version of this article (https://doi.org/10.1007/s11869-020-00811-z) contains supplementary material, which is available to authorized users.

✉ Elke Hertig
elke.hertig@med.uni-augsburg.de

[1] Regional Climate Change and Health, Faculty of Medicine, Augsburg University, Alter Postweg 118, 86159 Augsburg, Germany

methane volatile organic compounds. It has to be distinguished from stratospheric ozone, which acts to protect against harmful UV radiation. With respect to long-term O_3 exposure, an effect was found on respiratory and cardiorespiratory mortality, especially in people with potential predisposing conditions (WHO 2013). In a study of effects of short-term exposure to O_3, a 0.35% (95% confidence interval 0.12–0.58) increase in cardiovascular mortality per 10 μg/m^3 increase in daily maximum 1-h O_3 concentrations was found (Katsouyanni et al. 2009). For the protection of human health from O_3 exposure, information and alarm thresholds (1-h O_3 concentration of 180 μg/m^3 and 240 μg/m^3, respectively) and target values (maximum 8-h mean of 120 μg/m^3 at no more than 25 days per year) exist. The WHO (2006) even recommends the use of 100 μg/m^3 8-h mean as guideline. In a study relating myocardial infarction (MI) frequencies to O_3 exposure for the city of Augsburg, Bavaria, significantly enhanced MI frequencies were found above 96 μg/m^3 daily maximum 1-h O_3 concentration (Hertig et al. 2019).

There is also evidence of synergistic effects between temperature and O_3 pollution. Thus, health effects of O_3 are worse on hot days (Pattenden et al. 2010). Also, Katsouyanni and Analitis (2009) found that the effects of heat-wave days on mortality were larger at days with high O_3 concentrations, particularly in the age group 75–84 years.

Climate change is associated not only with an increase of mean temperature but also with an increase of temperature extremes in Europe (Jacob et al. 2014) and, via changes of the synoptic conditions and the chemical environment, of ground-level O_3 (Katragkou et al. 2011). Increases in summertime O_3 are assessed for mid-Europe until the end of the twenty-first century (Colette et al. 2015), particularly in polluted environments (Schnell et al. 2016). Changing patterns of disease are occurring in response to the changing environmental conditions (De Sario et al. 2013). With respect to changes of the temperature-mortality relationships under climate change, for Central Europe, a strong increase of excess mortality of 3.5% (95% confidence interval 0.4 to 7.1) under RCP8.5 scenario conditions was assessed (Gasparrini et al. 2017). A recent study by Orru et al. (2019), analysing changes of premature deaths due to temperature and O_3 exposure, found that under RCP4.5 scenario conditions future heat-related deaths will increase, while O_3-related deaths will increase when considering only climate change, but will decrease when assuming reductions in O_3 precursor emissions. In contrast, Hendriks et al. (2016) note that the effects of increasing temperatures on O_3 concentrations and associated health impacts might be higher than the reduction that is achieved by lowering ozone precursor emissions.

In summary, there are still few combined temperature and O_3 assessments relevant for human health and there is an incomplete picture about the future changes of temperature and O_3 exposure, particularly on the regional to local scale. Thus, the current contribution addresses relationships between air temperature and ground-level O_3. Local projections of temperature and ozone events under the constraints of ongoing climate change until the end of the twenty-first century are presented. Attention is also given to the change of health-relevant thresholds of these variables. The federal state of Bavaria, Southern Germany, builds the regional focus.

Data and data preparation

Since health-relevant higher air temperature and O_3 concentrations occur in Bavaria primarily in spring and summer, all analyses comprise the months from April to September.

Station-based air quality data

Station-based air quality data were provided by the Bavarian Environment Agency (Bayerischen Landesamt für Umwelt 2019). Twenty-nine air quality stations could be retrieved which provide daily ozone data with a minimum of 5 years of data. Name, geographic coordinates, height and time series length of each station are given in Table S1 in the Supplementary Material. From the hourly data, the daily maximum 1-h ozone concentration was derived. Preliminary analyses using the daily maximum 8-h average O_3 concentration or the daily mean O_3 concentration provided a lower performance in the statistical models. Thus, the daily maximum 1-h ozone concentration (O_{3max}) was chosen. Daily mean 1-h nitrogen oxide concentrations (NO_{mean}, NO_{2mean}) were also extracted to analyse the station-specific NO_x-O_3 relationships. Station characteristics were assumed from the classification of the Environment Agency, categorising into urban traffic (5 stations), urban background (6 stations), suburban background (10 stations), peri-urban background (3 stations) and rural regional background (4 stations) as well as rural remote background (1 station). The location of the stations as well as their station characteristic can be seen in Fig. 1.

Station-based air temperature data

Daily 2-m maximum air temperature (T_{max}) from meteorological stations of the German Weather Service (Deutscher Wetterdienst 2019) was also extracted. Temperature stations were selected to match the spatial location of the ozone stations as close as possible. Note that the meteorological stations are in general not located within the same station environment as the air quality stations. Meteorological measurements of the German Weather Service target at regional representativeness, where local influences should be minimised. Thus, temperature stations are located in urban proximity, but outside of high-density areas. Studies (e.g. Fenner et al. 2019) have shown that there are only minor effects of the urban heat island

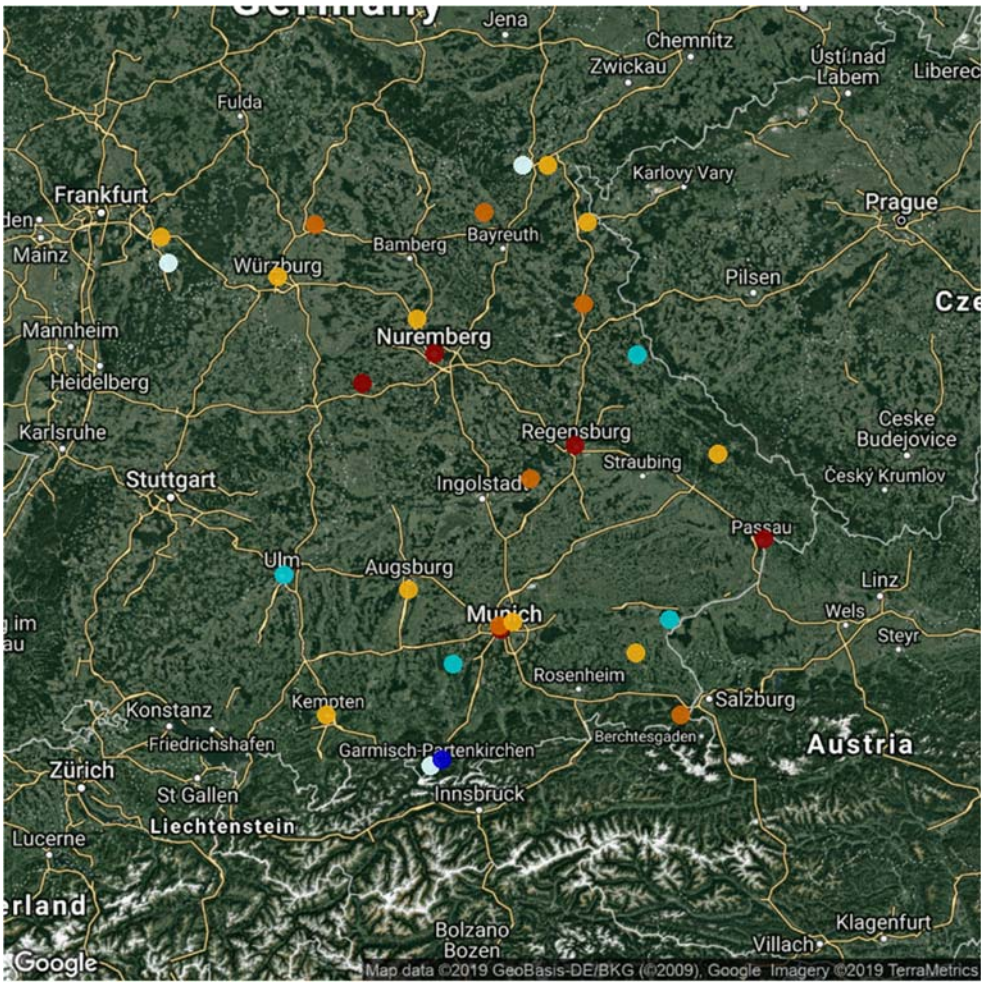

Fig. 1 Location of the air quality stations and their station characteristics (red: urban traffic, orange: urban background, yellow: suburban background, light blue: peri-urban background, turquoise: rural regional background, dark blue: rural remote background)

(UHI) on T_{max}, since the UHI is predominately a nocturnal phenomenon and thus mainly appears in increased minimum and mean air temperatures. Thus, it is assumed that there is no substantial urban-rural difference with respect to T_{max} and that the 29 stations can be regarded as representative for the particular city regions.

Predictor data from reanalysis

Larger scale predictor data, i.e. daily mean sea-level pressure data, as well as air temperature and humidity of the 850 hPa level, were taken in a 1° × 1° resolution from the European Centre for Medium-Range Weather Forecasts (ECMWF) ERA5 reanalysis (Hersbach and Dee 2016). The choice of predictor variables was governed by a literature review (e.g. Carro-Calvo et al. 2017; Otero et al. 2016), own analyses and the data availability in reanalysis and earth system models. Mean sea-level pressure data was derived for the domain 25°N–70°N, 25°W–40°E. For all predictors, the mean of the 9 grid boxes covering the area over and around the particular target city was used.

Air flow indices were calculated from the daily mean sea-level pressure fields based on an objective weather type approach developed by Jenkinson and Collison (1977). It has been advanced for reanalysis data, for instance by Jones et al. (2013). The approach makes use of three variables that define the circulation features over the region of interest: overall direction of air flow, the strength of flow and the total shear vorticity. A grid-point pattern, laid out over the study region, was used to calculate these wind-flow characteristics. Details on the calculation can be found in Jones et al. (2013). The indices were calculated for each of the 29 air quality stations using the geographic coordinates of the stations rounded to full degrees as central points for the definition of the grid-point pattern.

Earth system model (ESM) data

Historical and RCP8.5 scenario (Van Vuuren et al. 2011) runs performed for the Coupled Model Intercomparison Project round 5 (CMIP5) were downloaded from the CMIP5 archive (http://pcmdi9.llnl.gov/esgf-web-fe/). Model data were taken

from a three-member MPI-ESM-LR ensemble, and one member each from CMCC-CMS, IPSL-CM5A-LR and ACCESS 1-0. The same variables as for the ERA5 reanalysis have been extracted and interpolated to a 1°×1° resolution using ordinary kriging. The period 1950–2005 of the historical runs and the period 2006–2100 of the scenario runs are used.

Methods

Statistical downscaling models

For the definition of the appropriate statistical models, goodness of fit of the O_{3max} data and T_{max} data was tested. Normal, Gamma, Weibull and lognormal distributions were considered for O_{3max} and normal distribution for T_{max}. Since O_{3max} data contains some zero values, the O_{3max} minimum value was set to 1 μg/m^3 for hypothesis testing. Anderson-Darling test and Cramér-von Mises criterion are used for the selection of the statistical models.

Separate statistical models for O_{3max} and T_{max} as predictand were built. With the objective of consistent downscaling results, the same predictors were used for both target variables. Predictors-predictand relationships were assessed using generalised additive models (GAM; Wood 2017). GAM is a generalised linear model involving a sum of smooth functions of covariates for the linear predictor. Within GAM, non-linear as well as linear relationships can be modelled. As predictors, the mean of the 9 grid boxes over the target city of daily mean air temperature (x_1) and daily mean relative humidity(x_2), both at the 850 hPa level, as well as daily mean sea-level pressure(x_3), was used. Furthermore, the three air flow indices (x_4, x_5, x_6) were taken as predictors. Seasonality (defined by sin (2πd/365.25) and cos (2πd/365.25), x_7, x_8) was also taken into account. Preliminary tests with linear (x) as well as a non-linear ($f(x)$) characterisations of the relationships showed that non-linear characterisations are appropriate. Thus, the model can be written as

$$g(\mu_i) = A_i\theta + f_1(x_{1i}) + f_2(x_{2i}) + f_3(x_{3i}) + f_4(x_{4i}) + f_5(x_{5i}) + f_6(x_{6i}) + f_{78}(x_{7i,}x_{8i,}) \quad (1)$$

where $\mu_i \equiv E(Y_i)$ and Y_i $EF(\mu_i, \varnothing)$. Y_i is a response variable, EF(μ_i, ∅) is an exponential family distribution with mean μ_i and scale parameter ∅, A_i is a row of the model matrix for any strictly parametric model components, θ is the corresponding parameter vector and the f_i are smooth functions of the covariates x_k. Note that one smooth function of both seasonality parameters x_7, x_8 was chosen. In the present work, penalised thin plate regression splines were used for estimating the smooth functions. Thin plate regression splines avoid the problem of knot placement, can be constructed for smooths of multiple predictor variables and are relatively computationally efficient (Wood 2017).

Model performance

Performance of the statistical models was evaluated using the p values of the model coefficients, the adjusted R^2 of the model and the partial autocorrelation function of the residuals. Also, a bootstrap procedure was applied. Bootstrapping with random sampling of calibration (2/3 of data) and validation (1/3 of data) periods was performed using 100 random samples. Tests with sample sizes up to 5000 gave similar results; thus, 100 samples were selected to balance between stable results and high computer efficiency. Performance in calibration and validation was evaluated using the correlation coefficient between observed and modelled values as well as the mean squared error skill score (MSESS) with the long-term climatology as reference forecast. Both measures were evaluated as mean values over the 100 random samples.

Projections

Statistical projections were done by replacing reanalysis predictor data with the corresponding ESM data. Time slice differences under the RCP8.5 scenario conditions of the future periods 2041–2060 (mid- twenty-first century) and 2081–2100 (end twenty-first century), respectively, compared with the historical period 1986–2005 are used to illustrate the changes of O_{3max} and T_{max} under future climate change.

Linear scaling (e.g. Teutschbein et al. 2011; Casanueva et al. 2016) was applied to bias-correct O_{3max} and T_{max} statistically downscaled from ESM data. In this regard, monthly correction factors based on the difference of O_{3max} and T_{max}, assessed using historical ESM values and observed O_{3max} and T_{max} values, were applied so that ESM downscaled values matched the long-term monthly averages of the measured O_{3max} and T_{max}, respectively. Thus, biases between downscaled time series and observations were identified and then used to correct both historical and scenario runs, assuming stationarity of the relationships under historical and scenario conditions.

Uncertainties were assessed by using the 95% confidence interval of the GAM-modelled mean (based on the standard error of predictions within the GAM models), the range over the 100 statistical models and the range over the six ESM runs. Results are presented as ensemble mean change and its confidence range, using the maximum uncertainty range, i.e. the minimum and maximum of the change signals across the models obtained from the 95% confidence intervals of the 600 models (100 statistical models × 6 ESM runs).

Results

Characteristics, trends and health-related threshold exceedances of T_{max} and O_{3max}

The median value of T_{max} was 20.4 °C and the 95% quantile amounted to 28.4 °C, calculated as means over the 29 stations in the months from April to September. Daily T_{max} for each station as mean over the months from April to September can be seen in Fig. 2. As spatial pattern, a negative relationship of T_{max} with the altitude of the stations becomes visible. A correlation analysis using Spearman's rank correlation yielded a coefficient of − 0.79 between T_{max} and altitude. Due to the consideration of T_{max} (and not T_{mean} or T_{min}) and since the temperature stations are located outside urban centres ("Station-based air temperature data"), no UHI signal is present in the temperature data.

O_{3max} concentrations show distinct differences depending on the station characteristics. Thus, the median and the 95% quantile values from April to September, as means over the urban traffic stations, amounted to 77 μg/m^3 and 124 μg/m^3, respectively, but were already 92 μg/m^3 and 138 μg/m^3 for the urban, suburban and rural peri-urban background stations, and were even 98 μg/m^3 and 141 μg/m^3 for the stations of the rural regional background. Figure 3 provides an overview of daily mean O_{3max} for each station from April to September.

O_{3max} concentrations depend strongly on NO_x levels and (B) VOC ((biogenic) volatile organic compounds) availability. The median values were 25 μg/m^3 for NO_{mean} and 42 μg/m^3 for NO_{2mean} at the urban traffic stations from April to September. Concentrations decline fast towards the urban hinterland and amounted in the urban background to 7 μg/m^3 for NO_{mean} and 25 μg/m^3 for NO_{2mean}, and in the rural regional background only to 1 μg/m^3 and 9 μg/m^3, respectively. The relevance of spatial NO_x variations for O_3 formation can also be seen in correlation relationships. Thus, the correlation coefficient between O_{3max} and the (NO_{2mean}/NO_{mean}) ratio amounted to 0.45 at the urban traffic sites and dropped to around zero in the rural background. Also, the negative correlation coefficient between O_{3max} and NO_{mean} deteriorates from − 0.39 to around zero. It highlights the contribution of NO_x to ozone formation in the urban area as well as the process of ozone destruction at high NO concentrations. A similar analysis for (B) VOCs could not be done due to data non-availability.

There was a mean (non-significant) T_{max} warming trend of + 0.3 K/decade in the months April to September in the time period 1990–2017. For O_{3max}, there was no clear overall trend, with negative trend (e.g. rural regional background with − 2.4 μg/m^3 per decade), no trend (urban background) or positive trend (suburban background with 2 μg/m^3 per decade). In summary, a heterogeneous picture of O_{3max} progression

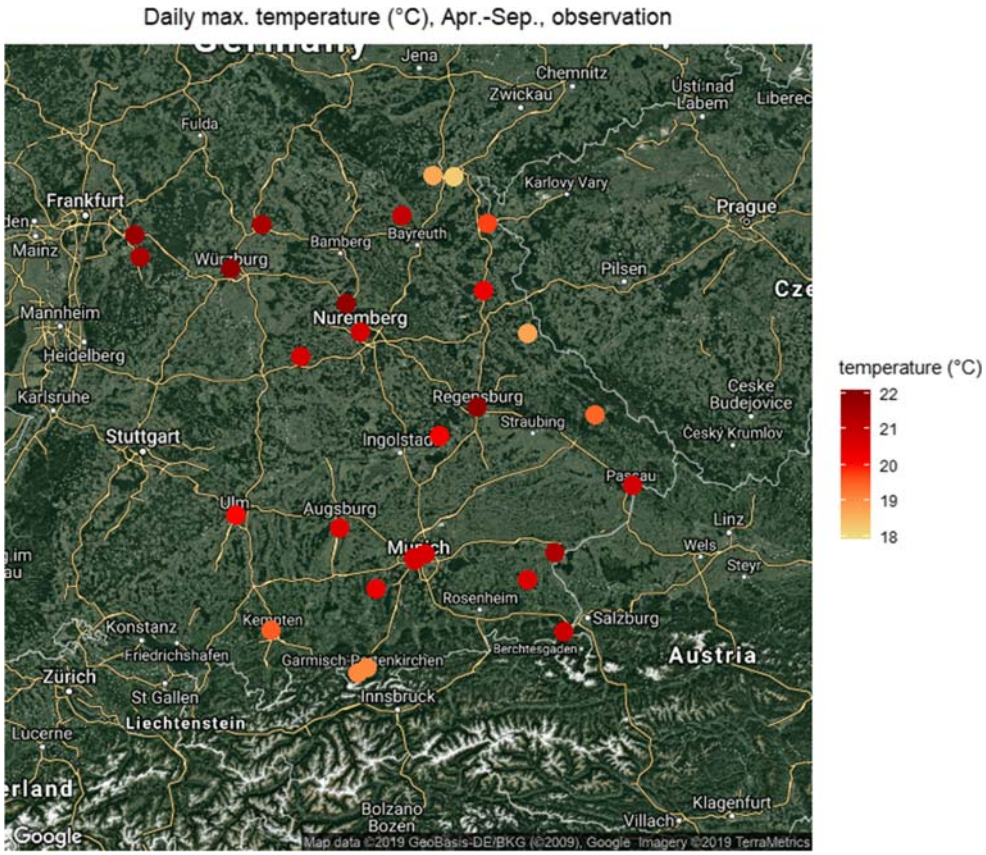

Fig. 2 Mean daily T_{max} in the months from April to September. Mean for each station over the years as indicated in Table S1

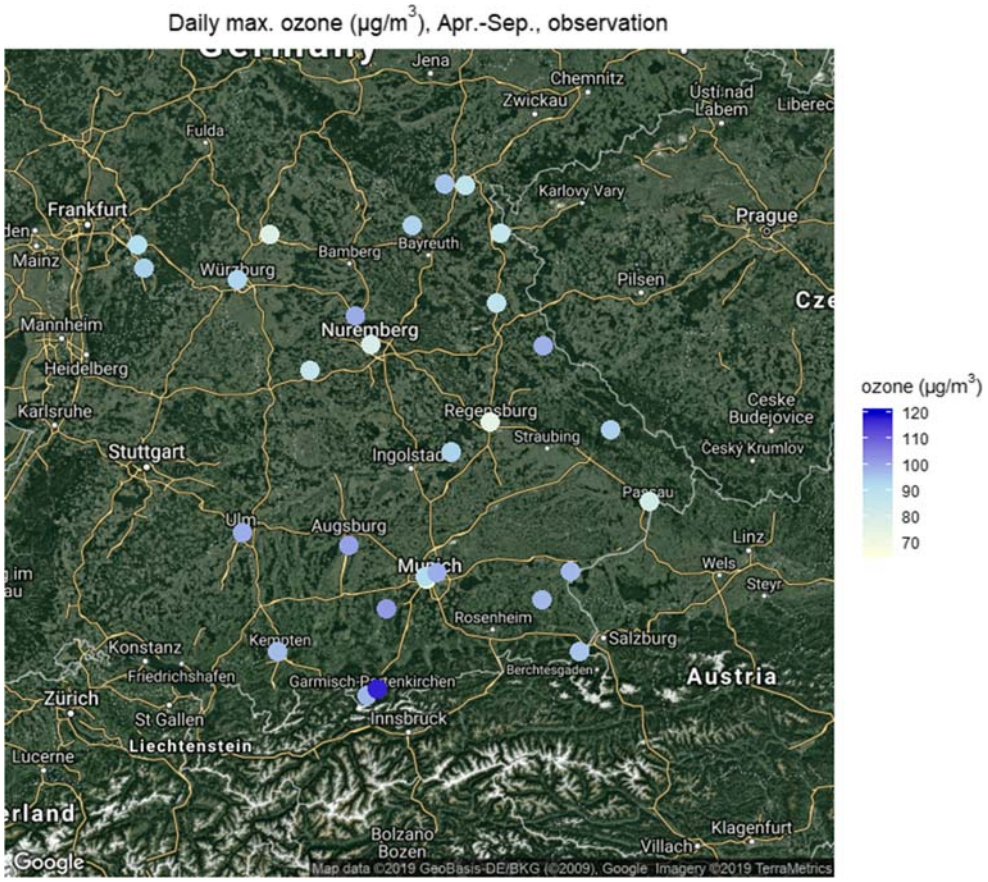

Fig. 3 Mean daily O_{3max} concentrations in the months from April to September. Mean for each station over the years as indicated in Table S1

becomes apparent, with no dependence on specific station characteristics. Note however that the given numbers refer to station group means calculated from stations with different time series lengths and that, for individual stations, different trends may have occurred.

Table 1 gives an overview of the frequency of threshold exceedances ($T_{max} > 30$ °C, $O_{3max} > 100$ µg/m^3/120 µg/m^3/180 µg/m^3) grouped according to station characteristics. Note that all O_3 thresholds were calculated using the daily 1-h maximum, not the maximum 8-h mean. The station associated with rural remote background conditions was not included in this statistic, since it is located in 1770 m asl and shows in general higher O_3 concentrations. O_3 degradation by deposition and titration, which are dominant processes in the boundary layer, plays only a minor role at this site. As expected, there was no urban-rural differentiation of hot days ($T_{max} > 30$ °C) and only small differences occurred across different station characteristics. With respect to health-relevant O_3 concentrations, a high frequency became apparent aside urban traffic sites. Already in the urban background, about one-third of all days between April and September showed O_{3max} concentrations above 100 µg/m^3, increasing to over 43% in the rural regional background. The threshold of 120 µg/m^3 was exceeded at about 15% of all days in background locations and very extreme O_3 days with values above 180 µg/m^3 occur in 0.3–0.4% of all days.

Table 1 Observed frequency of exceedance (% of days) of the thresholds $O_{3max} > 100$ µg/m^3/120 µg/m^3/180 µg/m^3 and $T_{max} > 30$ °C in the months April to September. Numbers are the mean over stations with similar station characteristic

Station characteristics	Number of stations	$T_{max} >$ 30 °C	$O_{3max} >$ 100 µg/m^3	$O_{3max} >$ 120 µg/m^3	$O_{3max} >$ 180 µg/m^3	$T_{max} >$ 30 °C and $O_{3max} >$ 100 µg/m^3
Urban traffic	5	5.3	19.2	7.7	0.1	4.6
Urban background	6	5.1	33.3	14.4	0.3	5.0
Suburban background	10	4.3	36.0	15.7	0.4	4.1
Rural peri-urban background	3	3.1	38.0	16.2	0.3	3.0
Rural regional background	4	4.1	43.4	18.8	0.4	4.0

In summary, there was a considerable exposure to ground-level ozone in the summer half year from April to September, with the exception of urban traffic sites. The occurrence of thermal load was almost always connected with the concurrent occurrence of O_3 pollution (Table 1). The combined thermal-O_3 pollution events affect in general the urban areas as well as the rural regions, with the highest frequency of combined events at urban background locations.

Relationships between O_{3max} and T_{max}

GAM models between O_{3max} and T_{max} revealed that there is in general a non-linear relationship between the two variables, with larger increases of O_{3max} at higher T_{max}. The explained variances from the GAM models amounted to about 50% as average across the 29 stations, highlighting the strong connection of O_{3max} concentrations with T_{max}. Figure 4 shows the relationship exemplarily for one station in Munich, located in the suburban background (München Johanneskirchen), but the same kind of relationship was found for all stations, independent of the station characteristics. As a consequence of the non-linear relationship, it can be expected that increases of T_{max} under future climate change conditions have a large impact on O_{3max} concentrations, particularly if the T_{max} rise lies in the range of associated large O_{3max} increases.

Statistical model performance and predictors

Goodness of fit tests showed for O_{3max} that the best fitting distribution was the Gamma distribution for 20 stations and the normal distribution for 9 stations. Thus, GAM based on Gamma distribution was applied to the 20 stations. As link function, the log link was used. For the remaining 9 stations, GAM based on normal distribution with identity link was applied. With respect to T_{max}, the best fitting distribution was the normal distribution and thus, GAM based on normal distribution (identity link) was chosen for this variable.

With respect to statistical model performance, the correlation coefficient between observed and modelled T_{max} as mean over the 100 random samples amounted between 0.95 and 0.97 in calibration and 0.94 and 0.97 in validation, depending on the station considered. The MSESS (with 0% = no model skill, 100% = perfect model) took values between 91 and 95% in calibration, and between 89 and 94% in validation.

For O_{3max}, the correlation coefficient between observed and modelled values spanned from 0.71 to 0.85 in calibration and 0.70 to 0.84 in validation, depending on the particular station considered. MSESS amounted to 50 up to 72% in calibration and between 50 and 70% in validation.

Station-based 2 m T_{max} showed a strong, almost linear relationship with mean temperature above the boundary layer in 850 hPa height. Also, T_{max} generally increased with increasing sea-level pressure, pointing to higher air temperatures under high-pressure conditions in the summer half year. High relative humidity values at the 850 hPa level indicated decreased ground-level T_{max} values, reflecting the general inverse relationship between relative humidity and temperature. Also, higher relative humidity values relate to more moist air, which is associated with development of clouds and precipitation and consequently with reduced 2 m T_{max}. Seasonality

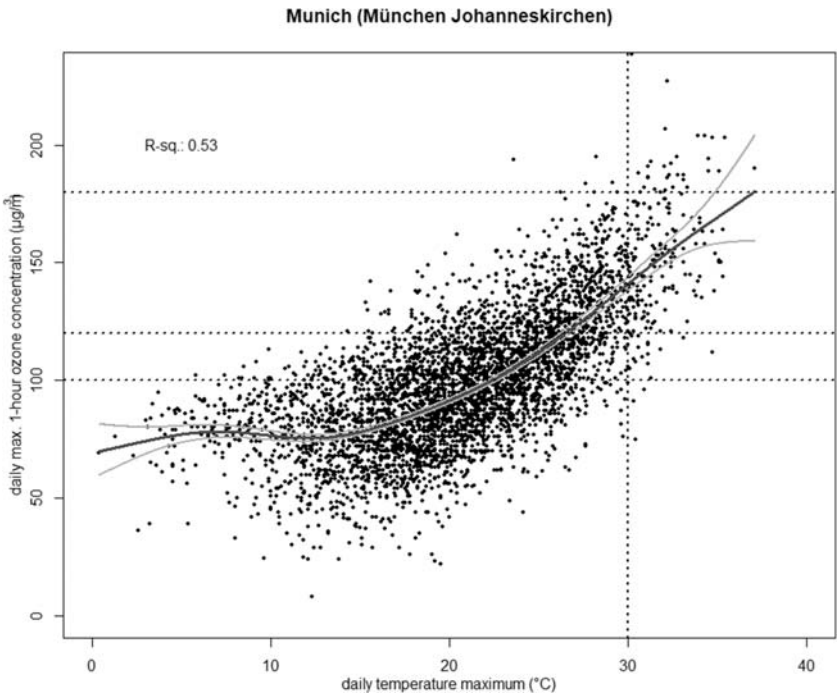

Fig. 4 Observation-based relationship between daily O_{3max} and daily T_{max} April–September 1993–2017 for Munich (München Johanneskirchen)

also played an important role in the GAMs, whereas the air flow indices had, depending on the station considered, a varying importance in the statistical models.

For O_{3max} as target variable, the significance of the larger scale predictors, as expressed by the *p* values of the model coefficients, varied across the stations, but for all stations, *p*-values were significant (95% level) for the predictor variables 850 hPa air temperature, 850 hPa relative humidity and seasonality. In general, station-based ground-level O_{3max} showed a non-linear relationship with daily mean air temperature of the 850 hPa level, with stronger increases of O_{3max} at higher temperatures. This non-linear relationship already became apparent in the connection between O_{3max} and station-based 2 m T_{max} ("Relationships between O_{3max} and T_{max}"). In contrast, high daily mean relative humidity values of the 850 hPa level were associated with low O_{3max} concentrations. High relative humidity may be seen as an indicator for enhanced cloudiness, reduced incoming solar radiation and atmospheric lability and thus implies reduced O_3 concentrations. Furthermore, high atmospheric humidity plays a role by the formation of secondary organic aerosols and by reducing the chemical reactivity of the system, particularly under low NO_x conditions (Hertig et al. 2019). With respect to the other predictor variables, a more diverse picture appeared, depending on the target station, but higher mean sea-level pressure was usually connected with increased O_{3max} concentrations. It points to the connection of O_3 built-up by photochemical reactions under high solar radiation in the presence of high-pressure systems. An increase of the total air flow often leaded to a decrease of O_{3max} concentrations. Increased wind speeds tend to disperse pollutants and can weaken ozone concentrations, whereas stagnant or low air flow favours pollution concentrations to build up. It can also be seen as an indicator that ozone was produced at the vicinity of the measurement station, and that longer range transport did not play a major role in these cases. The total shear vorticity (as an indicator for cyclonic/anticyclonic flow) showed complex relationships with O_{3max}. The relationship with the overall direction of flow also varied, due to the dependence of O_{3max} on sources and sinks in the upstream area.

Projections for the twenty-first century

Bias correction

There was a very low bias of T_{max} and O_{3max} between observed and with reanalysis-modelled values, indicating a good performance of the downscaling models per se. However, a comparison of the values statistically modelled using the historical ESM predictor data with reanalysis-modelled values revealed partly larger biases. While MPI-ESM-LR and CMCC-CMS showed a comparatively good agreement between reanalysis-modelled and ESM-modelled values, historically modelled values from IPSL-CM5A-LR were about 1.5 K warmer and values from ACCESS 1-0 even about 3 K warmer than reanalysis-modelled values. Thus, linear scaling was applied to the statistically downscaled values in order to minimise ESM-related biases. After linear scaling, the mean bias over all stations for T_{max} amounted to 0.27 K (with a bias range from 0.1 to 0.4 K, depending on the station considered), indicating that the T_{max} values modelled with historical ESM predictors were still somewhat warmer than observation-based T_{max} values after bias correction. Concerning the days with threshold exceedance of $T_{max} > 30$ °C, there was an about 1% overestimation of the frequency when using bias-corrected ESM historical predictors compared with observational data. For O_{3max}, the mean bias after linear scaling was 0.8 μg/m^3 (range from 0.1 to 2.2 μg/m^3), pointing to overall slightly higher O_{3max} in the modelled values using historical ESM data. With respect to threshold exceedances, the relative frequency of days with $O_{3max} > 100$ μg/m^3 was on average 4% overestimated in the ESM-modelled values compared with observational values, whereas the frequencies for the thresholds $O_{3max} > 120$ μg/m^3 and $O_{3max} > 180$ μg/m^3 were underestimated with − 0.8% and − 0.2%, respectively. Since in the observation-based/historical periods the frequency of co-occurring $T_{max} > 30$ °C and $O_{3max} > 100$ μg/m^3 events was mainly governed by the T_{max} frequency (i.e. a hot day was usually characterised by elevated O_3 concentrations), there was, as for the T_{max} frequency, an about 1% overestimation in the ESM historical assessments compared with observations.

Future changes of T_{max} and $O_{3\ max}$

Figure 5 shows the mean change of daily T_{max} between the scenario period 2081–2100 and the historical period 1986–2005, statistically downscaled under the RCP8.5 scenario assumptions. For each station, the value refers to the mean over 600 models (100 statistical models × 6 ESM runs). In addition, Table S2 (Supplementary Material) gives the uncertainty range defined by the minimum and maximum change values from the GAM 95% confidence intervals across the 100 statistical models and six ESMs. Thus, uncertainties related to statistical prediction errors, to the choice of calibration/validation periods and to the application of different ESMs were addressed. A north-south gradient of T_{max} warming until the end of the twenty-first century became apparent with stronger T_{max} increases in the southern parts of Bavaria compared with the northern parts (Fig. 5). The average T_{max} increase under the RCP8.5 scenario amounted to 2.3 K until the mid-twenty-first century (not shown) and to 5 K (to 4.4 K up to 6.3 K, depending on the station considered) until the end of the twenty-first century. This implies a mean rise of T_{max} from 20.7 °C in the historical period 1986–2005 to 25.7 °C in the scenario period 2081–2100. Even within the very

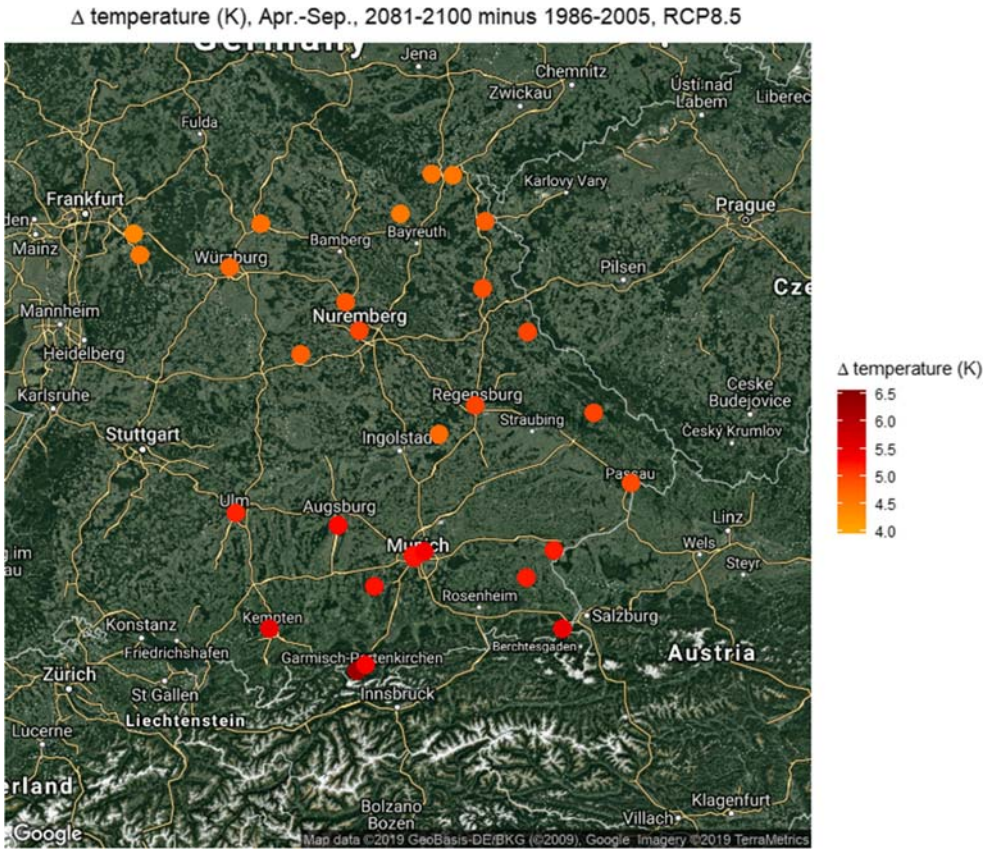

Fig. 5 Change of daily T_{max} from April to September between the periods 2081 to 2100 compared with 1986 to 2005 under RCP8.5 scenario

conservative lower bounds of the confidence ranges, the average increase was 2.8 K (range from 0.7 to 4 K, depending on the station considered, see Table S2), but in the worst-case (upper bounds of the confidence ranges) to 8.5 K (range from 7.3 to 10.5 K). Thus, the downscaling results indicate substantial increases of daily T_{max} from April to September and consequently of human thermal load in the future.

Concerning O_{3max}, Fig. 6 and Table S3 (Supplementary Material) give the mean changes and the uncertainty ranges for the scenario period 2081–2100 compared with the historical period 1986–2005, statistically downscaled under the RCP8.5 scenario assumptions. For all stations, an increase of daily O_{3max} in the months April to September emerged, ranging between about 13 and 22 μg/m^3 depending on the station considered. However, no dependence between the rate of increase and specific station characteristics became evident with the exception of the high-altitude rural remote background station Garmisch-Partenkirchen Wankgipfel, which exhibited the lowest increase. The average increase across all stations amounted to 17 μg/m^3 for the months April to September in the time period 2081–2100 (to 7 μg/m^3 for the time period 2041–2060, not shown). Thus, on average, an O_{3max} increase was projected from 93 μg/m^3 in the historical period 1986–2005 to 110 μg/m^3 until the end of the century. The lower and upper bounds of the confidence ranges gave a mean change between − 1 μg/m^3 (− 18 to 7 μg/m^3, depending on the station considered) and 52 μg/m^3 (34 to 86 μg/m^3). In summary, the lower bounds of the confidence ranges indicated no change of O_{3max} or slight decreases at some locations until the end of the century. However, the multi-model mean points towards an increase of O_{3max} at all stations and the upper bounds of the confidence ranges denote quite substantial increases of O_{3max} under ongoing climate change. Due to the strong relationship between ozone and temperature, a large part of the projected O_{3max} increases can directly be related to the temperature rise under future climate change.

With respect to the attribution of uncertainties, as expressed by the confidence ranges of the projection results, it became evident that uncertainties from the statistical models as well as the uncertainties related to the ESMs have about an equal share in total uncertainty.

In order to gain further insight into the impact of the projected T_{max} and O_{3max} changes on human health, Table 2 gives the assessed changes of health-relevant threshold exceedances ($T_{max} > 30$ °C, $O_{3max} > 100$ μg/m^3/120 μg/m^3/180 μg/m^3). A strong increase of hot days with $T_{max} > 30$ °C can be seen, leading to projected frequencies of about 30% of all days in the months from April to September at the end of the twenty-first century. With respect to the frequencies of days when $O_{3max} > 100$ μg/m^3 or $O_{3max} > 120$ μg/m^3, very sharp rises were assessed as well, leading to exceedances of $O_{3max} > 100$ μg/m^3 at about 40% of all days at urban traffic

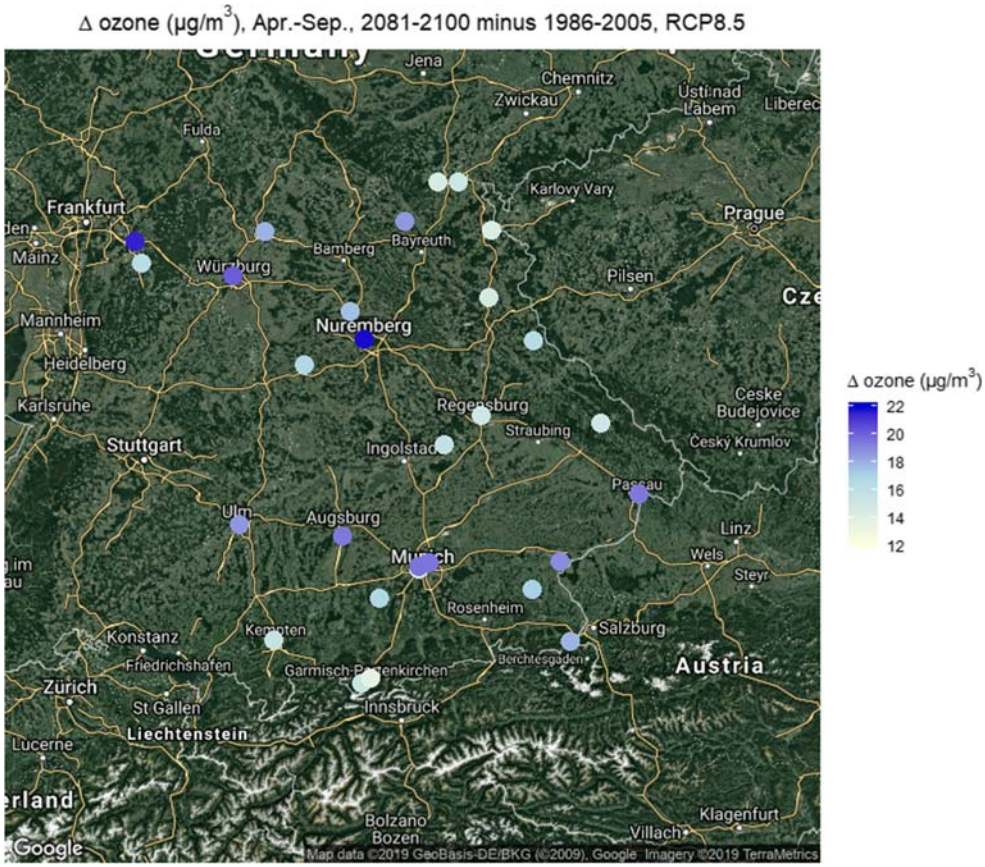

Fig. 6 Change of daily O_{3max} from April to September between the periods 2081 to 2100 compared with 1986 to 2005 under RCP8.5 scenario

sites and up to about 70% of all days in the rural regional background. Days with $O_{3max} > 120$ µg/m^3 were projected to occur still at about 20% of all days at urban traffic sites and about 45% in rural regional background locations. Besides, there was an overall increase of the frequency of very high O_{3max} concentrations ($O_{3max} > 180$ µg/m^3) to about 1.5–2.5% of all days assessed. Regarding the frequencies of combined T_{max} and O_{3max} events, there were also strong increases projected, with the increases being strongly connected to the advance of $T_{max} > 30$ °C frequencies. Only at urban traffic sites lower O_{3max} concentrations can limit the number of co-occurring events, whereas at hot days, O_{3max} concentrations always exceeded the threshold of 100 µg/m^3 (also of 120 µg/m^3, not shown) at all other station locations. Hence, the frequencies of $T_{max} > 30$ °C and $O_{3max} > 100$ µg/m^3 days in the future time slice 2081–2100 amounted to 27.5% at urban traffic sites to over 29% at urban background locations of all days in the months from April to September, indicating a substantial burden of health-relevant thermal load and ozone pollution in the future.

Table 2 Projected frequency of exceedance (% of days) of the thresholds $O_{3max} > 100$ µg/m^3/120 µg/m^3/180 µg/m^3 and $T_{max} > 30$ °C in the months April to September for the scenario period 2081–2100 (italicized numbers) and change in frequency compared with the historical period 1986–2005 (bold numbers in brackets). Numbers are the mean over stations with similar station characteristic

Station characteristics	Number of stations	$T_{max} >$ 30 °C	$O_{3max} >$ 100 µg/m^3	$O_{3max} >$ 120 µg/m^3	$O_{3max} >$ 180 µg/m^3	$T_{max} >$ 30 °C and $O_{3max} >$ 100 µg/m^3
Urban traffic	5	*31.2* (+**25.1**)	*40.9* (+**23.6**)	*21.5* (+**17.4**)	*1.6* (+**1.5**)	*27.5* (+**22.4**)
Urban background	6	*29.8* (+**23.5**)	*56.8* (+**22.1**)	*34.3* (+**23.1**)	*2.0* (+**1.9**)	*29.3* (+**23.1**)
Suburban background	10	*28.3* (+**22.8**)	*62.3* (+**21.7**)	*38.8* (+**24.1**)	*2.6* (+**2.4**)	*28.2* (+**22.8**)
Rural peri-urban background	3	*26.9* (+**22.2**)	*62.7* (+**20.6**)	*39.6* (+**23.1**)	*1.4* (+**1.3**)	*26.8* (+**22.1**)
Rural regional background	4	*28.0* (+**23.3**)	*69.4* (+**21.8**)	*44.7* (+**27.1**)	*1.7* (+**1.5**)	*28.0* (+**23.3**)

Discussion

Daily T_{max} and O_{3max} were assessed for 29 Bavarian locations with different air quality settings. Statistical downscaling models based on GAM were developed to assess the relationships between larger scale meteorological predictors and local-scale T_{max} and O_{3max} in the observational period. Subsequently, ESM data were integrated into the statistical models, and T_{max} and O_{3max} were projected until the end of the twenty-first century under the RCP8.5 scenario conditions. Uncertainty estimates of the downscaling results considered uncertainties related to statistical prediction errors within the GAMs, uncertainties covering the choice of different calibration/validation periods and uncertainties due to the application of different ESMs. Uncertainties from the statistical models as well as the uncertainties related to the ESMs contributed about equally to total uncertainty.

In the observational period, daily T_{max} in the months from April to September amounted to 20.4 °C and hot days with $T_{max} > 30$ °C occurred on average at about 4.4% of all days, pointing to the location of Bavaria in a rather temperate climate. Daily O_{3max} amounted at the background locations on average to over 90 μg/m^3. Furthermore, urban background locations exhibited about one-third of all days between April and September with O_{3max} concentrations above 100 μg/m^3, increasing to over 43% in the rural regional background. Still, about 15% of all days exceeded the threshold of 120 μg/m^3 at background locations. The frequency of co-occurring $T_{max} >$ 30 °C and $O_{3max} > 100$ μg/m^3 days amounted on average to approx. 4.1% and was mainly governed by the frequency of hot days, since high T_{max} was usually accompanied by elevated O_{3max} concentrations.

Under RCP8.5 scenario conditions, a substantial increase of T_{max} with a mean value of 5 K (uncertainty range from 2.8 to 8.5 K) in the period 2081–2100 compared with the period 1986–2005 was assessed. These results are largely consistent with other studies over the European area (e.g. Jacob et al. 2014). The frequency of days with $T_{max} > 30$ °C showed also a significant rise. Thus, under a strong climate change forcing, hot days may occur at about 30% of all days in the months from April to September.

Projections pointed also to increases of O_{3max}, with a mean rise of 17 μg/m^3 (uncertainty range spanning from − 1 to 52 μg/m^3). The frequency of threshold exceedances showed also large changes, with mostly over 20% increases of days with $O_{3max} > 100$ μg/m^3 and $O_{3max} > 120$ μg/m^3 at all station locations. Consequently, a very frequent exposure to ozone pollution occurs at background locations in the future and even at urban traffic sites, the frequency of $O_{3max} > 100$ μg/m^3 will rise to about 40% of all days. In recent years, increases of O_3 particularly at urban or suburban background sites were observed (Sicard et al. 2018; this study). Sicard et al. (2018) attributed the increasing levels in urban surroundings to a lower O_3 degradation by NO, due to the reduction in local NO_x emissions. Under climate change conditions, Schnell et al. (2016) found increases of mean and extreme O_3 in summer mainly in more polluted regions of Europe, North America and Asia. The authors concluded that higher temperatures increase the efficiency of precursors to produce O_3 in polluted regions, whereas precursor availability in neighbouring, downwind locations is reduced. In the present study, no obvious dependence of the O_3 increases from the station characteristics could be seen. In fact, regional O_3 pollution does not only depend on the availability of O_3 precursors, but changes of dynamical and photochemical processes are also important as well as there can be an impact from tropospheric background changes.

Conclusions

In general, a strong relationship between air temperature and O_3 formation was found. As a consequence, temperature can be regarded as a powerful predictor to assess O_3 concentrations. Due to the non-linear nature of the relationship, higher temperatures usually lead to substantially enhanced O_3 concentrations and temperature extremes were usually accompanied by high O_3 concentrations. Furthermore, temperature increases in the scope of climate change considerably affected future O_3 concentrations.

With respect to changes of T_{max}, O_{3max} and their specific thresholds as well as of combined $T_{max} > 30$ °C and $O_{3max} >$ 100 μg/m^3 events in the future, a sharp increase was projected, leading to an occurrence of such combined events at about 27–29% of all days in the summer months from April to September. The increases are mainly associated with the strong temperature rise until the end of the century. In summary, the projected T_{max} and O_{3max} changes point to a considerable increased health burden in Bavaria until the end of the century, resulting from strong changes of both variables and their associated individual and combined impact on human health.

Funding information Open Access funding provided by Projekt DEAL. This work was supported by the Deutsche Forschungsgemeinschaft (DFG, German Research Foundation) under project number 408057478.

Open Access This article is licensed under a Creative Commons Attribution 4.0 International License, which permits use, sharing, adaptation, distribution and reproduction in any medium or format, as long as you give appropriate credit to the original author(s) and the source, provide a link to the Creative Commons licence, and indicate if changes were made. The images or other third party material in this article are included in the article's Creative Commons licence, unless indicated otherwise in a credit line to the material. If material is not included in the article's Creative Commons licence and your intended use is not permitted by statutory regulation or exceeds the permitted use, you will

need to obtain permission directly from the copyright holder. To view a copy of this licence, visit http://creativecommons.org/licenses/by/4.0/.

References

Bayerischen Landesamt für Umwelt (2019) Messwertarchiv. https://www.lfu.bayern.de/luft/immissionsmessungen/messwertarchiv/index.htm (07.02.2019)

Carro-Calvo L, Ordóñez C, García-Herrera R, Schnell JL (2017) Spatial clustering and meteorological drivers of summer ozone in Europe. Atmos Environ 167:496–510

Casanueva A, Herrera S, Fernández J, Gutiérrez JM (2016) Towards a fair comparison of statistical and dynamical downscaling in the framework of the EURO-CORDEX initiative. Clim Chang 137(3–4): 411–426

Colette A, Andersson C, Baklanov A, Bessagnet B, Brandt J, Christensen JH, Doherty R, Engardt M, Geels C, Giannakopoulos C, Hedegaard GB, Katragkou E, Langner J, Lei H, Manders A, Melas D, Meleux F, Rouïl L, Sofiev M, Soares J, Stevenson DS, Tombrou-Tzella M, Varotsos KV, Young P (2015) Is the ozone climate penalty robust in Europe? Environ Res Lett 10(8):084015

De Sario M, Katsouyanni K, Michelozzi P (2013) Climate change, extreme weather events, air pollution and respiratory health in Europe. Eur Respir J 42(3):826–843

Deutscher Wetterdienst (2019) Climate Data Center. https://www.dwd.de/DE/klimaumwelt/cdc/cdc_node.html (07.02.2019)

Fenner D, Holtmann A, Krug A, Scherer D (2019) Heat waves in Berlin and Potsdam, Germany–Long-term trends and comparison of heat wave definitions from 1893 to 2017. Int J Climatol 39(4):2422–2437

Gasparrini A, Guo Y, Sera F, Vicedo-Cabrera AM, Huber V, Tong S, de Sousa Zanotti Stagliorio Coelho M, Nascimento Saldiva PH, Lavigne E, Matus Correa P, Valdes Ortega N, Kan H, Osorio S, Kyselý J, Urban A, Jaakkola JJK, Ryti NRI, Pascal M, Goodman PG, Zeka A, Michelozzi P, Scortichini M, Hashizume M, Honda Y, Hurtado-Diaz M, Cesar Cruz J, Seposo X, Kim H, Tobias A, Iñiguez C, Forsberg B, Åström DO, Ragettli MS, Guo YL, Wu CF, Zanobetti A, Schwartz J, Bell ML, Dang TN, van D, Heaviside C, Vardoulakis S, Hajat S, Haines A, Armstrong B (2017) Projections of temperature-related excess mortality under climate change scenarios. Lancet Planet Health 1(9):e360–e367

Hajat S, Kosatky T (2010) Heat-related mortality: a review and exploration of heterogeneity. J Epidemiol Community Health 64(9):753–760

Hendriks C, Forsell N, Kiesewetter G, Schaap M, Schöpp W (2016) Ozone concentrations and damage for realistic future European climate and air quality scenarios. Atmos Environ (2016), doi: https://doi.org/10.1016/j.atmosenv.2016.08.026

Hersbach H, Dee D (2016) ERA5 reanalysis is in production, ECMWF Newsletter, Vol. 147, p. 7, available at: https://www.ecmwf.int/en/newsletter/147/news/era5-reanalysis-production (10.05.2019)

Hertig E, Schneider A, Peters A, von Scheidt W, Kuch B, Meisinger C (2019) Association of ground-level ozone, meteorological factors and weather types with daily myocardial infarction frequencies in Augsburg, Southern Germany. Atmos Environ 217:116975

Jacob D, Petersen J, Eggert B, Alias A, Christensen OB, Bouwer LM, Braun A, Colette A, Déqué M, Georgievski G, Georgopoulou E, Gobiet A, Menut L, Nikulin G, Haensler A, Hempelmann N, Jones C, Keuler K, Kovats S, Kröner N, Kotlarski S, Kriegsmann A, Martin E, van Meijgaard E, Moseley C, Pfeifer S, Preuschmann S, Radermacher C, Radtke K, Rechid D, Rounsevell M, Samuelsson P, Somot S, Soussana J-F, Teichmann C, Valentini R, Vautard R, Weber B, Yiou P (2014) EURO-CORDEX: new high resolution climate change projections for European impact research. Reg Environ Change 14:563–578

Jenkinson AF, Collison FP (1977) An initial climatology of gales over the North Sea. Synoptic Climatology Branch Memorandum No. 62, Meteorological Office, Bracknell

Jones PD, Harpham C, Briffa KR (2013) Lamb weather types derived from reanalysis products. Int J Climatol 33(5):1129–1139

Katragkou E, Zanis P, Kioutsioukis I, Tegoulias I, Melas D, Krüger BC, Coppola E (2011) Future climate change impacts on summer surface ozone from regional climate-air quality simulations over Europe. J Geophys Res Atmos 116(D22). https://doi.org/10.1029/2011JD015899

Katsouyanni K, Analitis A (2009) Investigating the synergistic effects between meteorological variables and air pollutants: results from the European PHEWE, EUROHEAT and CIRCE projects. Epidemiology 20(6):S264

Katsouyanni K, Samet JM, Anderson HR, Atkinson R, Le AT, Medina S, Samoli E, Touloumi G, Burnett RT, Krewski D, Ramsay T, Dominici F, Peng RD, Schwartz J, Zanobetti A, HEI Health Review Committee (2009) Air pollution and health: a European and north American approach (APHENA). Res Rep Health Eff Inst 142:5–90

Orru H, Astrom C, Andersson C, Tamm T, Ebi KL, Forsberg B (2019) Ozone and heat-related mortality in Europe in 2050 significantly affected by changes in climate, population and greenhouse gas emissions. Environ Res Lett 14(7): 074013

Otero N, Sillmann J, Schnell JL, Rust HW, Butler T (2016) Synoptic and meteorological drivers of extreme ozone concentrations over Europe. Environ Res Lett 11(2):024005

Pattenden S, Armstrong B, Milojevic A, Heal MR, Chalabi Z, Doherty R, Barratt B, Sari Kovats R, Wilkinson P (2010) Ozone, heat and mortality: acute effects in 15 British conurbations. Occup Environ Med 67(10):699–707

Schnell JL, Prather MJ, Josse B, Naik V, Horowitz LW, Zeng G, Shindell DT, Faluvegi G (2016) Effect of climate change on surface ozone over North America, Europe, and East Asia. Geophys Res Lett 43(7):3509–3518

Sicard P, Agathokleous E, Araminiene V, Carrari E, Hoshika Y, De Marco A, Paoletti E (2018) Should we see urban trees as effective solutions to reduce increasing ozone levels in cities? Environ Pollut 243:163–176

Song X, Wang S, Hu Y, Yue M, Zhang T, Liu Y, Tian J, Shang K (2017) Impact of ambient temperature on morbidity and mortality: an overview of reviews. Sci Total Environ 586:241–254

Teutschbein C, Wetterhall F, Seibert J (2011) Evaluation of different downscaling techniques for hydrological climate-change impact studies at the catchment scale. Clim Dyn 37(9–10):2087–2105

Van Vuuren DP, Edmonds J, Kainuma M, Riahi K, Thomson A, Hibbard K, Hurtt GC, Kram T, Krey V, Lamarque J-F, Masui T, Meinshausen M, Nakicenovic N, Smith SJ, Rose SK (2011) The representative concentration pathways: an overview. Clim Chang 109:5–31

Vescovi L, Rebetez M, Rong F (2005) Assessing public health risk due to extremely high temperature events: climate and social parameters. Clim Res 30(1):71–78

WHO (World Health Organization) (2013) Review of evidence on health aspects of air pollution –REVIHAAP project. Technical Report, World Health Organization, Copenhagen, 302 p

WHO (World Health Organization) (2006) Air quality guidelines: global update 2005: particulate matter, ozone, nitrogen dioxide, and sulfur dioxide. World Health Organization

Wood SN (2017) Generalized additive models: an introduction with R. Chapman and Hall/CRC, Boca Raton

Publisher's note Springer Nature remains neutral with regard to jurisdictional claims in published maps and institutional affiliations.